Unclassified

SECURITY CLASSIFICATION OF THIS PAGE (When Data Entered)

REPORT DOCUMENTATION PAGE		READ INSTRUCTIONS BEFORE COMPLETING FORM
1. REPORT NUMBER RPI Math. Rep. No. 159	2. GOVT ACCESSION NO.	3. RECIPIENT'S CATALOG NUMBER
4. TITLE (and Subtitle) On the Calculation of Acoustic Intensity Fluctucations caused by Ocean Currents		5. TYPE OF REPORT & PERIOD COVERED Technical Report 6. PERFORMING ORG. REPORT NUMBER
7. AUTHOR(s) M. J. Jacobson, W. L Siegmann, and J. S. Robertson		8. CONTRACT OR GRANT NUMBER(s) N00014-86-K-0129
9. PERFORMING ORGANIZATION NAME AND ADDRESS Rensselaer Polytechnic Institute Troy, New York 12180-3590		10. PROGRAM ELEMENT, PROJECT, TASK AREA & WORK UNIT NUMBERS NR 4254007
11. CONTROLLING OFFICE NAME AND ADDRESS Office of Naval Research, Code 1125 Department of the Navy Arlington, Virginia 22217		12. REPORT DATE 15 September, 1986 13. NUMBER OF PAGES 13
14. MONITORING AGENCY NAME & ADDRESS(if different from Controlling Office)		15. SECURITY CLASS. (of this report) 15a. DECLASSIFICATION/DOWNGRADING SCHEDULE

16. DISTRIBUTION STATEMENT (of this Report)

This document has been approved for public release and sale; its distribution is unlimited.

17. DISTRIBUTION STATEMENT (of the abstract entered in Block 20, if different from Report)

18. SUPPLEMENTARY NOTES

19. KEY WORDS (Continue on reverse side if necessary and identify by block number)

Underwater Acoustics
Environmental Acoustics
The Parabolic Approximation
Ocean Currents

20. ABSTRACT (Continue on reverse side if necessary and identify by block number) Ocean currents can cause significant and interesting effects on the intensity of underwater sound transmissions. We study this phenomenon via the parabolic approximation, beginning with conservation laws, and derive a family of equations, each of which is valid for different magnitudes of current speed, current gradient, and sound-speed variation. Numerical results indicate that some current structures can cause large variations in received intensity, and that substantial differences can occur in reciprocal transmissions. Current effects on intensity may be quite sensitive to the sound-speed distribution.

DD FORM 1 JAN 73 1473 EDITION OF 1 NOV 65 IS OBSOLETE
S/N 0102-LF-014-6601

Unclassified

SECURITY CLASSIFICATION OF THIS PAGE (When Data Entered)

On the Calculation of Acoustic Intensity Fluctuations caused by Ocean Currents

by

M. J. Jacobson, W. L. Siegmann
and J. S. Robertson

Department of Mathematical Sciences
Rensselaer Polytechnic Institute
Troy, New York 12180-3590

RPI Math. Rep. No. 159
September 15, 1986

This work was sponsored by
Code 1125, Office of Naval Research
Contract NO. N00014-86-K-0129
NR 4254007

ON THE CALCULATION OF ACOUSTIC INTENSITY FLUCTUATIONS CAUSED BY OCEAN CURRENTS

J.S. Robertson+, M.J. Jacobson*, and W.L. Siegmann*

+Department of Mathematics, U. S. Military Academy, West Point, NY, USA 10996-1788

*Department of Mathematical Sciences, Rensselaer Polytechnic Institute, Troy, NY, USA, 12180-3590

ABSTRACT

Ocean currents can cause significant and interesting effects on the intensity of underwater sound transmissions. We study this phenomenon via the parabolic approximation, beginning with conservation laws, and derive a family of equations, each of which is valid for different magnitudes of current speed, current gradient, and sound-speed variation. Numerical results indicate that some current structures can cause large variations in received intensity, and that substantial differences can occur in reciprocal transmissions. Current effects on intensity may be quite sensitive to the sound-speed distribution.

INTRODUCTION

Ocean currents cause interesting and significant effects on underwater sound. For example, in a time-independent ocean environment, currents cause reciprocity relations to fail. Based on ray theory, work has been done by the authors and others to model the influences of currents on acoustic transmissions. It has been shown, for instance, that certain current structures can cause large fluctuations in total-field intensity and per ray phase. These results are limited to high-frequency sound transmissions. To estimate current-induced effects for lower frequencies, a full-wave model should be used. One computational model is the parabolic approximation, which has been implemented using several algorithms, and is a particularly attractive method for efficiently generating transmission-loss calculations.

MODEL FORMULATION

In a complicated medium such as a moving ocean, it is not obvious how known parabolic equations should be modified to include current effects. For this reason, we systematically reformulated the governing time-dependent wave equation, starting from the conservation laws and state relations governing the ocean medium, and including medium motion (Robertson et al., 1985). If the current is assumed steady but non-uniform, additional terms occur in the wave equation. These terms depend on the current gradient and, as will be discussed below, can be significant in subsequent approximations.

We then assume that the sound source is time-harmonic and that the propagating wave is outgoing, thereby obtaining a reduced wave equation. After transforming coordinate systems, we invoke the far-field approximation, and proceed to generate a family of parabolic equations. Each of these equations depends on the relative sizes of three dimensionless parameters: a Mach number, the sound-speed deviation, and a shear number. The last parameter indicates the magnitude of current gradient, and also depends on source frequency. For example, a parabolic approximation appropriate for an isospeed sound channel, through which flows a steady depth-dependent current, is

$$2i\kappa_0\psi_r + \psi_{zz} - 2\kappa_0^2\left(\frac{u}{c_0}\right)\psi + \left(\frac{2}{c_0}\right)\left(\frac{du}{dz}\right)\psi_z = 0, \tag{1}$$

where κ_0 is a wave number, u is current speed, and ψ is an envelope of acoustic pressure in the far field. The reference sound speed c_0 in this isospeed case is equal to the sound speed c. Depth is indicated by z and range by r. It can be shown that range-dependent sound-speed profiles can be incorporated into these approximations in a straightforward way, provided that the horizontal gradient of sound speed is not large, which is often the case in many important ocean regions. For example, for a sound channel in which the sound-speed deviation is of the same order of magnitude as the Mach number, the appropriate equation is

$$2i\kappa_0\psi_r + \psi_{zz} + \kappa_0^2(n^2-1)\psi - 2\kappa_0^2\left(\frac{u}{c_0}\right)\psi + \left(\frac{2}{c_0}\right)\left(\frac{du}{dz}\right)\psi_z = 0, \tag{2}$$

where $n(r,z) = c_0/c$ is the index of refraction.

In Eqs. (1) and (2), the term which depends on the first derivative of current may or may not be retained, depending upon the size of the shear-number parameter. In the event that it is kept, the parabolic approximations are not in a "standard form"; that is, they cannot be solved directly with existing numerical implementations. However, it is possible to transform this family into related parabolic equations which <u>are</u> in a standard form. The transformed version of Eq. (2) is, for example:

$$2i\kappa_0\phi_r + \phi_{zz} + \kappa_0^2(n^2-1)\phi - 2\kappa_0^2\left(\frac{u}{c_0}\right)\phi - \frac{1}{c_0}\left(\frac{d^2u}{dz^2}\right)\phi - \frac{1}{c_0^2}\left(\frac{du}{dz}\right)^2\phi = 0, \tag{3}$$

where

$$\psi(z,r) = e^{-Mu(z)}\phi(z,r). \tag{4}$$

Note the appearance of two new terms in Eq. (3) which depend on the square of the derivative of current and the second derivative of current. The structure of Eq. (3) and other such equations suggests the use of an effective sound-speed profile (ESSP), which includes all sound-speed and current-related effects, and is used as the "actual" sound speed for numerical solution of the equations. For example, the ESSP corresponding to Eq. (3) is

$$\tilde{c} = c + u + \frac{1}{2\kappa_0^2 c_0}\left(\frac{du}{dz}\right)^2 + \frac{1}{2\kappa_0^2}\left(\frac{d^2u}{dz^2}\right). \tag{5}$$

NUMERICAL RESULTS

To solve any of our parabolic equations numerically, we elect to use the IFD model developed by Lee and Botseas (1982). In the discussion below, we consider several sound-speed profiles, together with current profiles, as

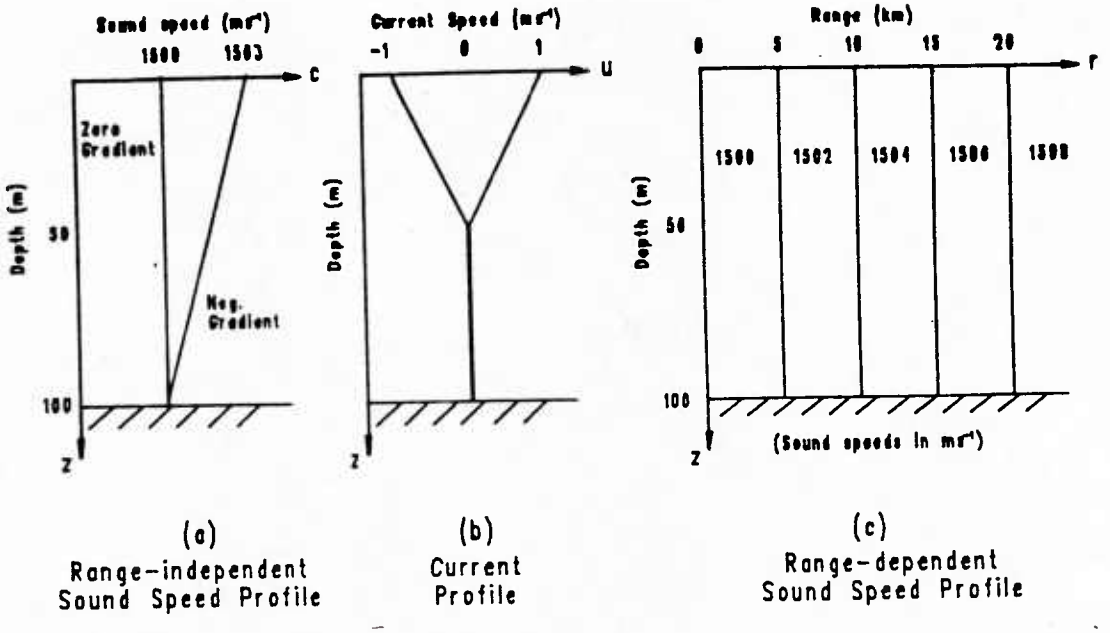

Fig. 1. Profiles of (a) range-independent sound speed, (b) current, and (c) range-dependent sound speed.

shown in Fig. 1. The zero-gradient and negative-gradient sound-speed profiles are sometimes range-independent as in Fig. 1(a), as are the current profiles in Fig. 1(b). The surface current may be either plus or minus 1 m/s. At other times, we employ a simple range-dependent sound-speed profile, Fig. 1(c), for which the horizontal gradient is both constant and small. Here, isopleths are vertical lines. We consider first the result of one calculation done in the isospeed channel, with surface current of magnitude 1 m/s. The source frequency is 200 Hz, for which it can be shown that current-gradient effects are negligible. The source and receiver depths are 25 m. In Figs. 2-6, the bottom acoustical properties are the same as in Robertson et al. (1985). Figure 2 shows a relative intensity in decibels versus range for three cases: no current present, a positive current in the source-receiver direction, and a negative current in the opposite direction. Several important current-related effects can be seen in the figure. When compared to the solid curve, representing intensity in the absence of any current, we see that a current with either direction can induce substantial variations in intensity. For example, with a positive current present, variations can exceed 10 dB over certain range intervals, such as those between 13 and 14 km. Similar behavior is seen for negative current. Current effects in both cases tend to increase with increasing range.

Intensity variations are highlighted in Fig. 3, which illustrates difference in relative intensity versus range for three cases: no current and positive current, no current and negative current, and positive and negative currents. Because source and receiver are at the same depth, this figure also illustrates one type of effect which may be seen in reciprocal transmissions (RTs). The intensity difference between positive and negative currents, indicated in Fig. 3 by the long-dashed curve, suggests that measurements of intensity variation between reciprocal source-receiver pairs may be very large. Near ranges 14 and 19 km, this difference attains a magnitude of nearly 20 dB. At other range intervals the difference is smaller, but significant. For example, between 10 and 12 km, the intensity difference is seen to generally be well over 4 dB. RT differences can also be significant in range-dependent channels. Using the sound-speed profile in Fig. 1(c), and the same source frequency, source-receiver depths, and current structure as above, the computed intensity difference between a source-receiver pair is shown in Fig. 4. Note that one effect of the range

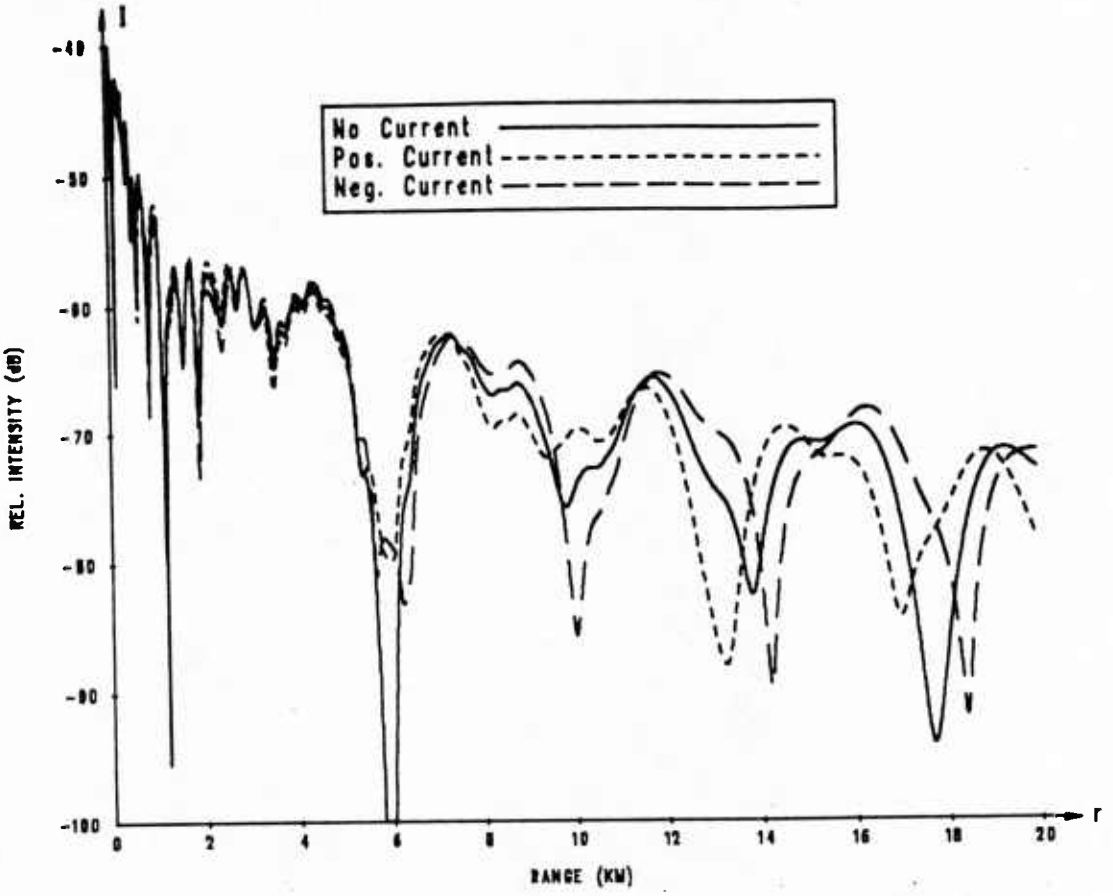

Fig. 2. Relative intensity versus range for three currents in an isospeed channel.

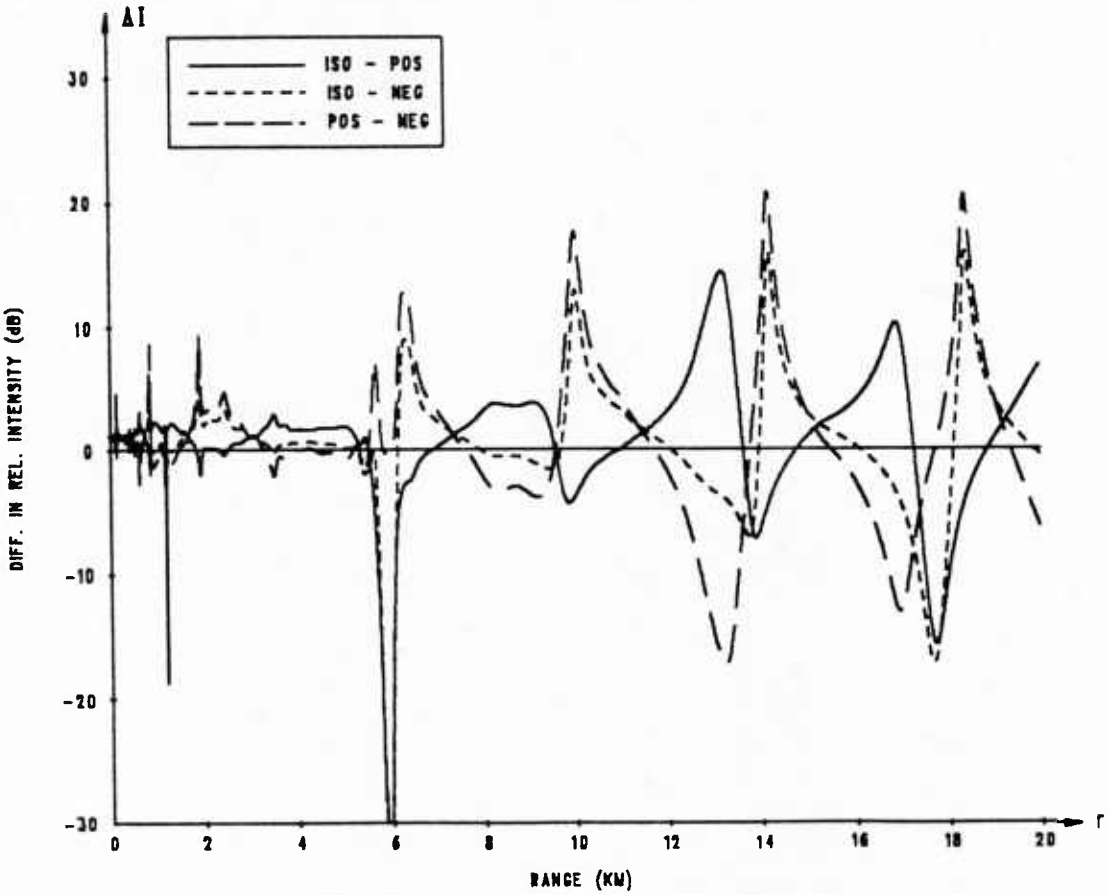

Fig. 3. Difference in relative intensity versus range, from Fig. 2. Oppositely-signed current effects are readily compared (long-dashed curve).

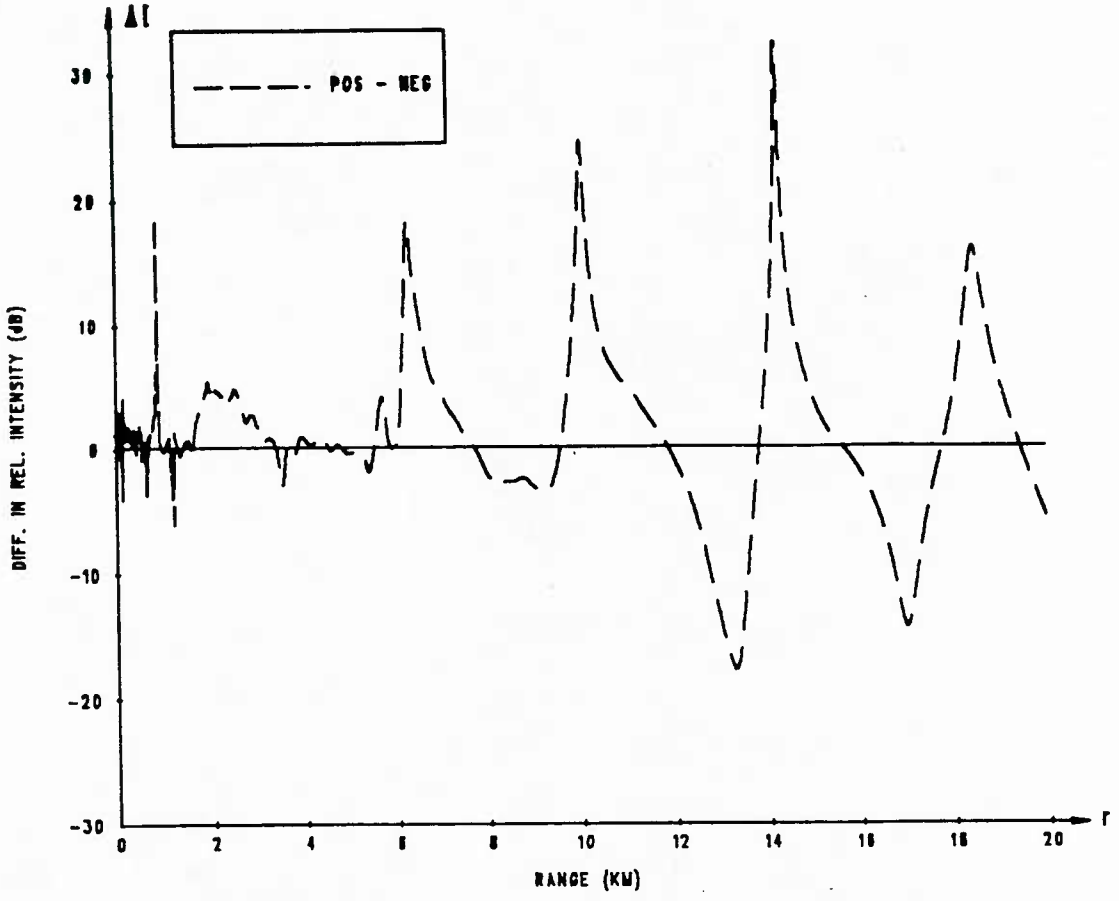

Fig. 4. Difference in relative intensity versus range, for current reversal. Reciprocal-transmission difference is shown for a range-dependent sound-speed profile.

variation in sound speed is to cause the relative intensity curve to shift toward the source, when compared to the analogous curve in Fig. 3. Maximum intensity values have been altered, also. For example, at a range 14 km, the peak difference is over 30 dB.

Another way to visualize the effects of reversing current direction is shown in Fig. 5. Here, differences in the two intensity functions are plotted as level curves in a portion of the depth-range plane. The difference is intensity for a positive current (in the source-receiver direction) minus intensity for a negative current, as in Fig. 1(b). The source frequency and source depth are again 200 Hz and 25 m, respectively. Contour intervals are 5 dB, with negative differences denoted by dotted curves. This figure illustrates the intensity differences that might be observed in a channel with tidal effects. At ranges larger than about 7 km, bottom attenuation has stripped away most higher modes, leaving a well-defined pattern of alternating intensity differences. Regions of large positive difference occur in finger-like patterns which alternately emanate from the channel surface and bottom. Similar structures are also seen for negative differences. In this example, a zone of very small differences extends in range across most of the channel at roughly mid-depth. Regions of maximum difference occur regularly above and below this zone. In contrast, the intensity-difference pattern in a negative gradient channel is noticeably different. Figure 6 shows the analogous level curves for the negative gradient profile of Fig. 1(a). The finger-like structures apparent in Fig. 5 have in some cases blended together in Fig. 6, leaving regions of high intensity difference located at many mid-depth points. The overall pattern is more complicated than the one present in the isospeed channel. Consequently, the intensity-difference pattern resulting from oppositely-signed currents

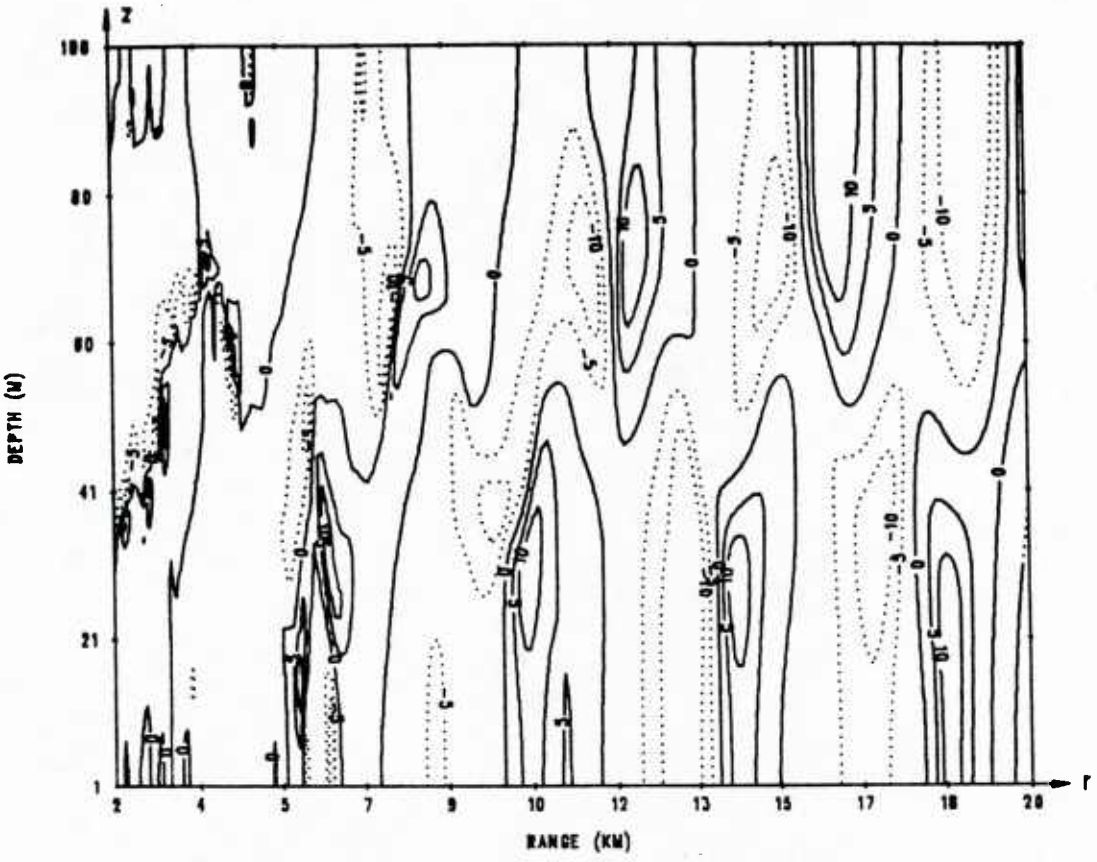

Fig. 5. Level curves of intensity difference in an isospeed channel, with current reversal.

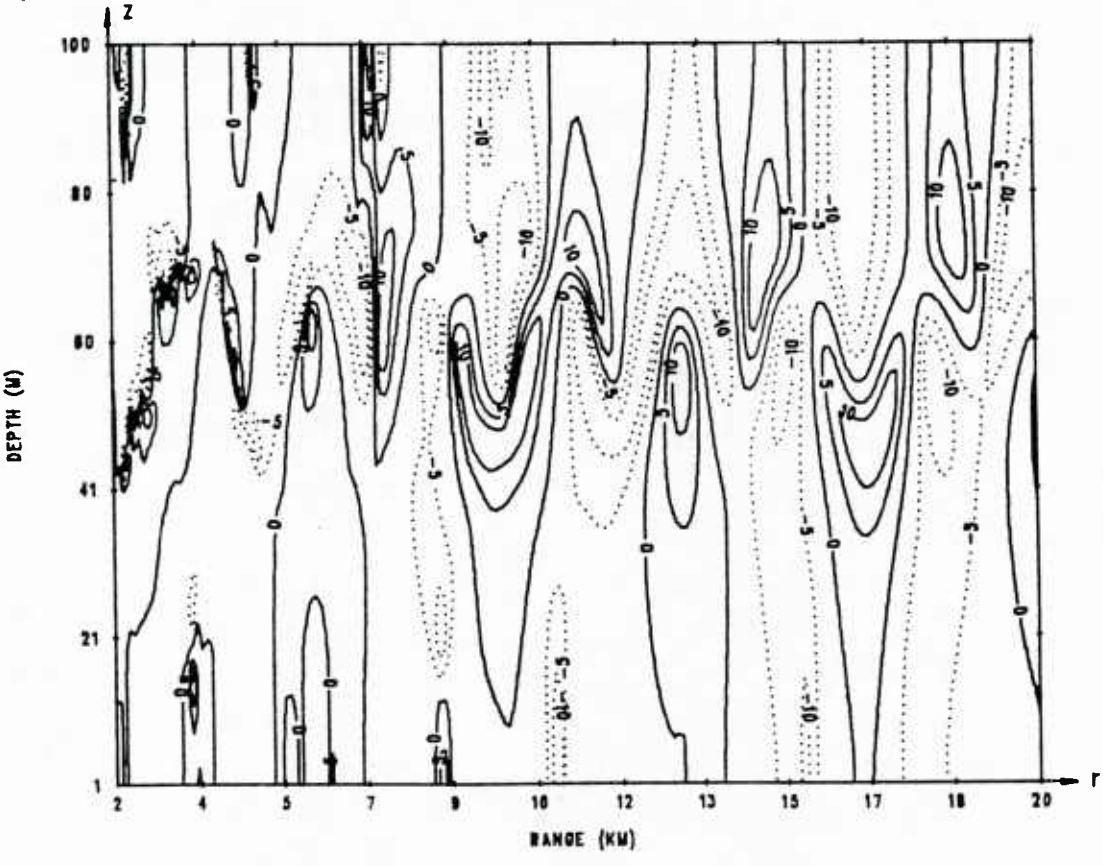

Fig. 6. Level curves of intensity difference for a negative gradient channel (see Fig. 1(a)), with current reversal.

appears to be very sensitive to these types of changes in the sound-speed profile.

For some current structures and lower source frequencies, the appropriate transformed parabolic equation will include new terms which depend on current concavity and (possibly) the square of current gradient. One type of current structure which may require additional terms is shown in Fig. 7(a). At the surface, the current speed is 1 m/s, and it decays to zero at the bottom. Note the appearance of several strong shear layers, particularly those at depths 35 and 60 m. The vertical shear structure seen here can be acoustically significant for sufficiently low source frequencies. For example, when the source frequency is 30 Hz, the ESSP is similiar to that given by Eq. (5) and is depicted in Fig. 7(b). In this example, concavity effects are significant, but shear effects can be neglected. Note that current concavity dominates the behavior of the ESSP. The current shear structure has introduced large rapid variations, one of which, at the depth 60 m, approaches 20 m/s in Fig. 7(b). For higher source frequencies, the magnitude of the variations decreases, yet may still be significant. We anticipate that this current structure can cause interesting acoustical effects.

In Fig. 8, we see one result of computations done with the current structure shown in Fig. 7(a). In order to observe concavity (or second derivative) effects, we solved the relevant parabolic equation, first with concavity included and then with concavity omitted. The root-mean-square difference of the intensities in the two cases, called J, was then calculated with a range averaging. Source and receiver depths are 25 m, and the source frequency is 100 Hz. The results for three different bottom types are shown. The rigid bottom is perfectly reflecting, while beneath the water column for the hard and soft bottoms is a second fluid layer with different sound speed and density. The hard bottom has larger discontinuities in these quantities than the soft bottom. For both hard and soft bottoms, a small amount of volume attenuation was introduced. As the bottom changes

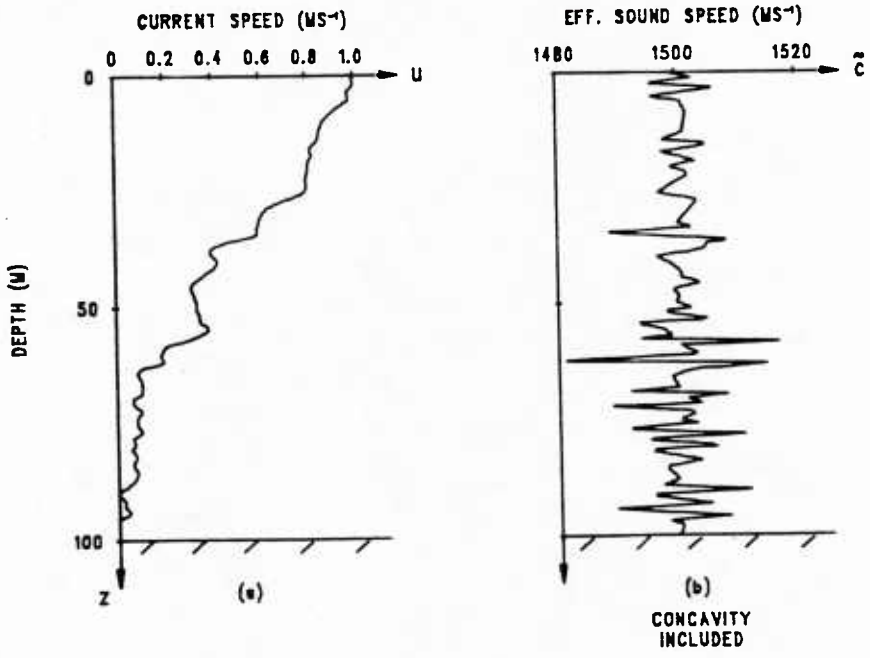

Fig. 7. Profiles of (a) a current with high shear, and (b) the effective sound speed.

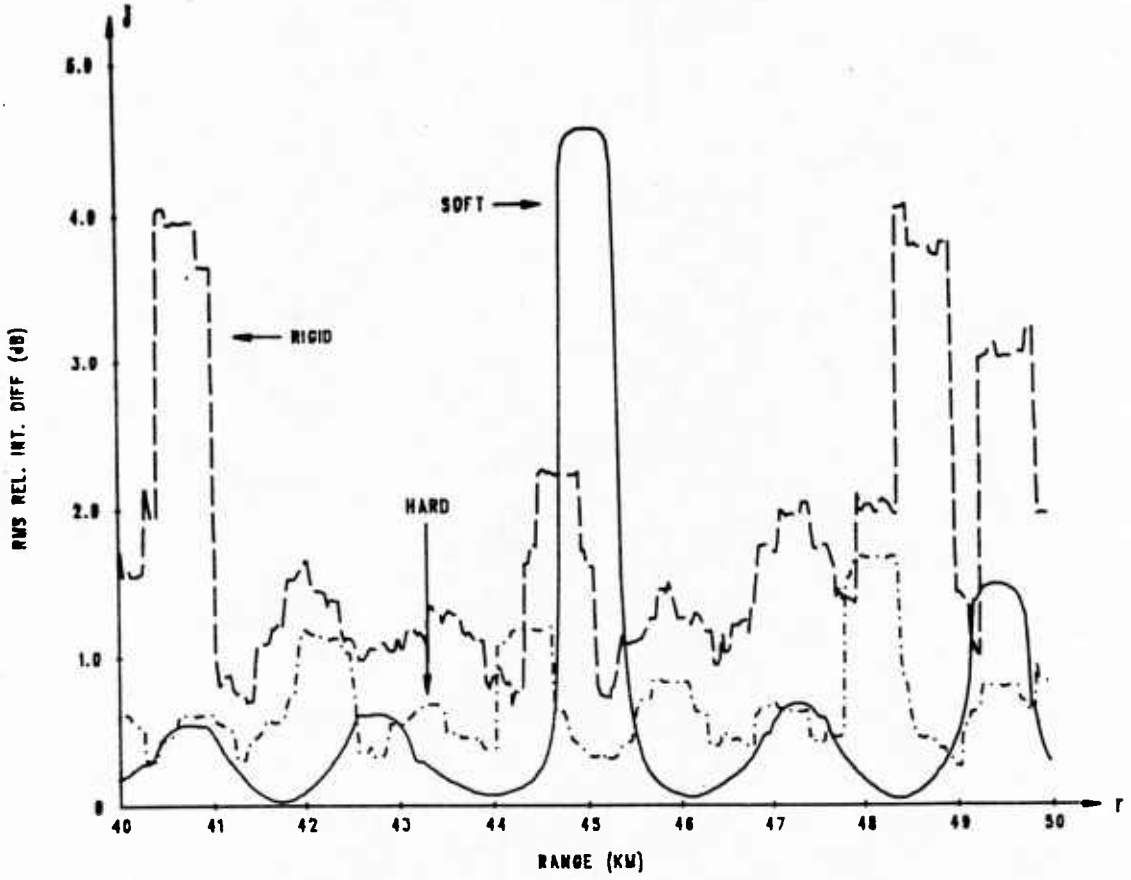

Fig. 8. RMS difference in intensity versus range for the current of Fig. 7(a) and for three bottom types.

from rigid to hard to soft, note that the overall values of J tend to decrease. However, the peak values may actually increase substantially. For example, at 45 km the soft bottom has a peak which is about 4 dB larger than its overall value. Furthermore, the curves are smoother for both the hard and soft bottoms, since they attenuate higher modes more rapidly than the rigid bottom. These observations illustrate the strong dependence of concavity effects on bottom influences in underwater sound transmissions.

SUMMARY

We discuss a family of parabolic approximations, valid for depth- and range-dependent sound-speed profiles, which include effects caused by steady depth-dependent currents. These approximations permit examination of intensity effects caused by currents for frequencies and environments where other models may not be valid or convenient. Using a standard numerical implementation, we present the results of computations for several current and sound-speed structures. They suggest that currents can cause significant intensity variations, principally by altering the effective sound-speed profile. Intensity differences arising from reciprocal transmissions are shown to be especially large. Also, current effects on intensity can be very sensitive to small changes in sound speed. Finally, the presence of current fine structure can introduce additional fluctuations in intensity predictions.

Lee, D., and Botseas, G., 1982, IFD: An implicit finite difference computer model for solving the parabolic equation, New London Lab., NUSC, New London, CT, TR 6659.

Robertson, J.S., Siegmann, W.L., and Jacobson, M.J., 1985, Current and current shear effects in the parabolic approximation for underwater sound channels, J. Acoust. Soc. Am., 77:1768.

UNCLASSIFIED
DISTRIBUTION LIST
DEC 1981

Addressee	No. of Copies
Office of Naval Research 800 North Quincy Street Arlington, Virginia 22217	
Attn: Code 425AC	2
102	1
102C	1
210	1
220	1
Office of Naval Technology 800 North Quincy Street Arlington, Virginia 22217	
Attn: MAT 0721	1
MAT 0724	1
Director Naval Research Laboratory 4555 Overlook Avenue, SW. Washington, D.C. 20375	
Attn: Dr. J. C. Munson	1
Mr. R. R. Rojas	1
Dr. B. B. Adams	1
Dr. W. B. Moseley	1
Dr. J. P. Dugan	1
Unclassified Library	1
Superintendent Naval Research Laboratory Underwater Sound Reference Division P.O. Box 8337 Orlando, Florida 32806	1
Director Office of Naval Research Branch Office 1030 East Green Street Pasadena, California 91106	1
Office of Naval Research Rm 239, Campbell Hall University of California Berkeley, California 94720	1
Director Office of Naval Research Branch Office 495 Summer Street Boston, Massachusetts 02210	1
Office of Naval Research New York Area Office 715 Broadway - 5th Floor New York, New York 10003	1
Commanding Officer Office of Naval Research Branch Office Box 39 FPO New York 09510	1
Director Office of Naval Research Branch Office 536 South Clark Street Chicago, Illinois 60605	1
Office of Naval Research Resident Representative University District Building, Room 422 1107 North East 45th Street Seattle, Washington 98105	1

Addressee	No. of C
Technical Director Naval Oceanographic Research and Development Activity NSTL Station Bay St. Louis, Mississippi 39522	
Attn: Technical Director	1
Dr. L. Solomon	1
Dr. R. Gardner	1
Mr. E. Chaika	1
Mr. R. Van Wyckhouse	1
Dr. S. W. Marshall	1
Director Naval Oceanographic Office NSTL Station Bay St. Louis, Mississippi 39522	
Attn: Mr. H. Beck	1
Dr. T. M. Davis	1
Mr. W. H. Geddes	1
Dr. W. Jobst	1
Mr. R. Merrifield	1
Mr. R. A. Peloquin	1
Dr. M. K. Shank	1
Office of the Assistant Secretary of the Navy for Research, Engineering and Systems Washington, D.C. 20350	
Attn: Dr. D. Barbe, Rm 4E732 Pentagon	1
Dr. J. H. Probus, Rm 5E779 Pentagon	1
Chief of Naval Operations Room 5D580, Pentagon Washington, D.C. 20350	
Attn: OP951F	1
Commander Naval Sea Systems Command Department of Navy Washington, D.C. 20362	
Attn: Capt. James M. Van Metre PMS 409	1
Chief of Naval Operations Office of the Director Naval Oceanographic Division OP-952 Department of the Navy Washington, D.C. 20352	
Attn: Dr. R. W. James	1
Capt. J. C. Harlett	1
Commander Oceanographic System, Atlantic Box 100 Norfolk, Virginia 23511	1
Commander Oceanographic System, Pacific Box 1390 Pearl Harbor, Hawaii 96860	1

Addressee	No. of Copies
Defense Advanced Research Projects Agency 1400 Wilson Boulevard Arlington, Virginia 22209 Attn: Capt. V. Simmons	1
ARPA Research Center Moffett Field Unit #1 California 94035 Attn: Mr. E. Smith	1
Commanding Officer Fleet Weather Central Box 113 Pearl Harbor, Hawaii 96860	1
Naval Ocean Systems Center (Kaneohe) Kaneohe, Hawaii 96863 Attn: Mr. D. Hightower Mr. B. Kishimoto Mr. R. Buecher	1 1 1
Commander Naval Electronic Systems Command 2511 Jefferson Davis Highway National Center #1 Arlington, Virginia 20360 Attn: CAPT C. A. Rose,, PME 124 LCDR P. Girard, NAVELEX 612	2
Commander Naval Air Systems Command Jefferson Plaza #1 1411 Jefferson Davis Highway Arlington, Virginia 20360	1
Commander Naval Sea Systems Command National Center #2 2521 Jefferson Davis Highway Arlington, Virginia 20362 Attn: SEA 63R 63Y	1 1
Commanding Officer Fleet Numerical Weather Central Monterey, California 93940 Attn: Mr. Paul Stevens Dr. D.R. McLain (NMFS)	1 1
Defense Documentation Center Cameron Station Alexandria, Virginia 22314	12
Commander Naval Ocean Systems Center Department of the Navy San Diego, California 92132 Attn: Dr. Daniel Andrews Dr. Dean Hanna Mr. Henry Aurand Dr. Harry A. Schenck	1 1 1 1

Addressee	No. of
Commander Naval Surface Weapons Center Acoustics Division Silver Spring, Maryland 20910	1
Commander Naval Surface Weapons Center Science and Mathematics Research Group (K05) Dahlgren, Virginia 22448 Attn: Dr. E.W. Schwiderski	1
Commanding Officer Naval Underwater Systems Center New London Laboratory New London, Connecticut 06320 Attn: Dr. William Von Winkle Dr. A. Nuttall Mr. A. Ellinthorpe Dr. D.M. Viccione Mr. A. Donn Cobb	1 1 1 1 1
Commander Naval Air Development Center Department of the Navy Warminster, Pennsylvania 18974 Attn: Unclassified Library	1
Commanding Officer Naval Coastal Systems Laboratory Panama City, Florida 32401 Attn: Unclassified Library	1
Commanding Officer Naval Underwater Systems Center Newport Laboratory Newport, Rhode Island 02840 Attn: Unclassified Library	1
Commander David W. Taylor Naval Ship Research and Development Center Bethesda, Maryland 20084 Attn: Dr. M. Sevik	1
Superintendent Naval Postgraduate School Monterey, California 93940	1
Superintendent U.S. Naval Academy Annapolis, Maryland 21402 Attn: Library	1
Commanding Officer Naval Intelligence Support Center 4301 Suitland Road Washington, D.C. 20390 Attn: NISC 20	1
Director Applied Physics Laboratory University of Washington 1013 North East 40th Street Seattle, Washington 98105 Attn: Dr. T.E. Ewart Dr. M. Schulkin	1 1

Addressee	No. of Copies
Applied Research Laboratories University of Texas at Austin P.O. Box 8029 10000 FM Road 1325 Austin, Texas 78712	
Attn: Dr. Loyd Hampton	1
Dr. Charles Wood	1
Atlantic Oceanographic and Meteorological Laboratories 15 Rickenbacker Causeway Miami, Florida 33149	
Attn: Dr. John Proni	1
Bell Telephone Laboratories 1 Whippany Road Whippany, New Jersey 07981	
Attn: Dr. Bruce Bogart	1
Dr. Peter Hirsch	1
Bolt, Beranek, and Newman, Inc. 50 Moulton Street Cambridge, Massachusetts 02238	
Attn: Dr. K. L. Chandiramani	1
Chase, Inc. 14 Pinckney Street Boston, Massachusetts 02114	
Attn: Dr. David Chase	1
Dr. David Middleton 127 East 91st Street New York, New York 10028	1
Duke University Department of Electrical Engineering Durham, North Carolina 27706	
Attn: Dr. Loren Nolte	1
General Electric Company Heavy Military Electronic Systems Syracuse, New York 13201	
Attn: Mr. Don Winfield	1
General Electric Company P.O. Box 1088 Schenectady, New York 12301	
Attn: Dr. Thomas G. Kincaid	1
Gould, Incorporated Chesapeake Instrument Division 6711 Baywaedow Drive Glen Burnie, Maryland 21061	
Attn: Dr. O. Lindemann	1
G R Associates, Inc. 10750 Columbia Pike Suite 602 Silver Spring, Maryland 20901	
Attn: Dr. Sheldon Gardner	
Dr. Frank Rees	
Hughes Aircraft Company P.O. Box 3310 Fullerton, California 92634	
Attn: Mr. S. W. Autrey	1

Addressee	No. of Cop.
Hydroacoustics, Inc. 321 Northland Ave. P.O. Box 3818 Rochester, New York 14610	1
Institute for Acoustical Research Miami Division for the Palisades Geophysical Institute 615 South West 2nd Avenue Miami, Florida 33130	
Attn: Mr. M. Kronengold	1
Dr. J. Clark	1
Institute of Geophysics and Planetary Physics Scripps Institute of Oceanography University of California La Jolla, California 92093	
Attn: Dr. W. Munk	1
Mr. J. Spiesberger	1
Jaycor Incorporated 205 South Whiting Street Suite 607 Alexandria, Virginia 22304	
Attn: Dr. S. Adams	1
Massachusetts Institute of Technology Acoustics and Vibration Laboratory 70 Massachusetts Avenue Room 5-222 Cambridge, Massachusetts 02139	
Attn: Professor Patrick Leehey	1
Palisades Sofar Station Bermuda Division of Palisades Geophysical Institute FPO New York 09560	
Attn: Mr. Carl Hartdegen	1
Polar Research Laboratory 123 Santa Barbara Avenue Santa Barbara, California 93101	
Attn: Mr. Beaumont Buck	1
Research Triangle Institute Research Triangle Park Durham, North Carolina 27709	
Attn: Dr. S. Huffman	1
Rensselaer Polytechnic Institute Troy, New York 12181	
Attn: Dr. Melvin J. Jacobson	
Science Applications, Inc. 8400 Westpark Drive McLean, Virginia 22102	
Attn: Dr. P. Tatro	
S.D.P. Inc. 15250 Ventura Boulevard Suite 518 Sherman Oaks, California 91403	
Attn: Dr. M. A. Basin	1

AOS:222:716:maf
79u222-346

Addressee	No. of Copies
Texas Instruments, Inc. 13500 North Central Expressway Dallas, Texas 75231 Attn: Mr. Charles Black	1
Underwater Systems, Inc. 8121 Georgia Avenue Silver Spring, Maryland 20910 Attn: Dr. H. Weinstein	1
University of Miami Rosenstiel School of Marine and Atmospheric Sciences 4600 Rickenbacker Causeway Miami, Florida 33149 Attn: Dr. H. DeFerrari	1
University of Michigan Department of Aerospace Engineering, North Campus Ann Arbor, Michigan 48109 Attn: Dr. W. W. Wilmarth	
University of Michigan Cooley Electronics Laboratory Ann Arbor, Michigan 48105 Attn: Dr. T. G. Birdsall	
University of Rhode Island Department of Electrical Engineering Wakefield, Rhode Island 02881 Attn: Dr. Donald Tufts	1
Woods Hole Oceanographic Institution Woods Hole, Massachusetts 02543 Attn: Dr. Paul McElroy Dr. R. Spindel	1 1